*J. Fluid Mech.* (1995), *vol.* 287, *pp.* 151–171



# The formation mechanism and shedding frequency of vortices from a sphere in uniform shear flow

By HIROSHI SAKAMOTO AND HIROYUKI HANIU
Department of Mechanical Engineering, Kitami Institute of Technology, Kitami, 090 Japan

(Received 26 January 1993 and in revised form 21 October 1994)

Experiments to investigate the formation mechanism and frequency of vortex shedding from a sphere in uniform shear flow were conducted in a water channel using flow visualization and velocity measurement. The Reynolds number, defined in terms of the sphere diameter and approach velocity at its centre, ranged from 200 to 3000. The shear parameter $K$, defined as the transverse velocity gradient of the shear flow non-dimensionalized by the above two parameters, was varied from 0 to 0.25. The critical Reynolds number beyond which vortex shedding from the sphere occurred was found to be lower than that for uniform flow and decreased approximately linearly with increasing shear parameter. Also, the Strouhal number of the hairpin-shaped vortex loops became larger than that for uniform flow and increased as the shear parameter increased.

The formation mechanism and the structure of vortex shedding were examined on the basis of series of photographs and subsequent image processing using computer graphics. The range of Reynolds number in the present investigation, extending up to 3000, could be classified into three regions on the basis of this study, and it was observed that the wake configuration did not differ substantially from that for uniform flow. Also, unlike the detachment point of vortex loops in uniform flow, which was irregularly located along the circumference of the sphere, the detachment point in shear flow was always on the high-velocity side.

## 1. Introduction

Wakes behind spheres are encountered so frequently in engineering applications that a considerable amount of research has been conducted and massive data have been accumulated. In particular, many reports which are concerned mainly with the vortex shedding from a sphere have been published (Möller 1938; Cometta 1957; Magarvey & Bishop 1961; Achenbach 1974; Pao & Kao 1977; Taneda 1978; Kim & Durbin 1988; Sakamoto & Haniu 1990). As described in their reports, Kim & Durbin (1988) and Sakamoto & Haniu (1990) have performed experiments on the vortex shedding frequency of a sphere over a wide Reynolds number range, and they found two distinct modes of unsteadiness which were associated with the small-scale instability of the separating shear layer and with the large-scale instability of the wake. In particular, they demonstrated that the higher frequency was detected only in the immediate downstream region of the sphere when the Reynolds number exceeded 800. Also, Taneda (1978) and Achenbach (1974) have demonstrated that there exist strong periodic fluctuations in the wake right up to the critical Reynolds number of $3 \times 10^5$. Studies have also been carried out on the formation mechanism and structure of vortex shedding from a sphere in a uniform flow. Magarvey & Bishop classified the observed

wake configuration into six distinct categories: single thread, double thread, wavy, vortex loop, vortex ring and asymmetrical wake. In particular, it was demonstrated that when a Reynolds number of about 300 is reached, the vortex rings begin to oscillate, and the wake forms hairpin-shaped vortex loops (Magarvey & MacLatchy 1965; Levi 1980; Sakamoto & Haniu 1990).

Most of these studies are concerned with vortex shedding from a sphere immersed in uniform flow, and no cases in which the vortex shedding from a sphere immersed in non-uniform flow in such a way that the free-stream velocity varies in the direction normal to it have been investigated so far. There have been a few studies on the drag and lift acting on a sphere immersed in such non-uniform flows; however, all of these studies except an analytical work of Auton (1987) are concerned with the drag and lift on the sphere below the critical Reynolds number where periodic vortex shedding occurs (Bretherton 1962; Saffman 1965; O'Neill 1968; Dandy & Dwyer 1990). No visual observations have so far been reported of the wake of a sphere in non-uniform flow.

The vortex shedding frequency of a sphere immersed in non-uniform flow is not only of interest as a topic in hydrodynamics but also of importance for practical cases involving the motion of a particle in a non-uniform flow, such as an air bubble flowing past a nearby wall, solid particles in pipes for pneumatic conveying, and the snow particles in blowing snow near the surface of the ground. Since the motion of these particles depends upon the wake fluctuation caused by the vortex shedding, it is important to know whether the presence of shear in the approaching stream has much of an effect on the mechanism by which the vortices are shed. Another case of a sphere immersed in non-uniform flow concerns the laminar-to-turbulent transition of the boundary layer. Hall (1967) examined the transition induced by small bluff bodies, including spheres, which were suspended at various heights above a flat surface within a developing boundary layer. He concluded that the mechanism by which the laminar-to-turbulent transition occurred was dependent upon the stability characteristics of the wake of the suspended body rather than the stability characteristics of the boundary layer. Thus, it is important to know the shedding conditions and detailed characteristics of vortices generated behind a sphere in non-uniform flow. The details of the behaviour of vortices, however, are still very much in question.

The purpose of the present paper is to clarify the vortex shedding frequency and wake structures of a sphere immersed in uniform shear flow. The Reynolds number, which is defined in terms of the sphere diameter and approach velocity at its centre, varied from 200 to 3000. Also, the shear parameter, defined as the transverse velocity gradient of the shear flow, non-dimensionalized by the approaching velocity and sphere diameter, varied from 0 to 0.25. First, the dependence of the vortex shedding frequency on the Reynolds number and shear parameter is examined in detail. Secondly, the formation mechanism and structure of the vortices shed from the sphere are examined on the basis of series of photographs and image-processing methods using computer graphics. Finally, the relationship between the wake configuration and the vortex shedding frequency of the sphere is closely examined.

## 2. Experimental arrangements

### 2.1. *Experimental apparatus*

Experiments were performed in a recirculating water channel, as shown in figure 1(*a*). The test section of the channel was rectangular in shape and had a width of 29 cm, depth of 30 cm, and length of 1.0 m. The surface of the test section was a free surface;

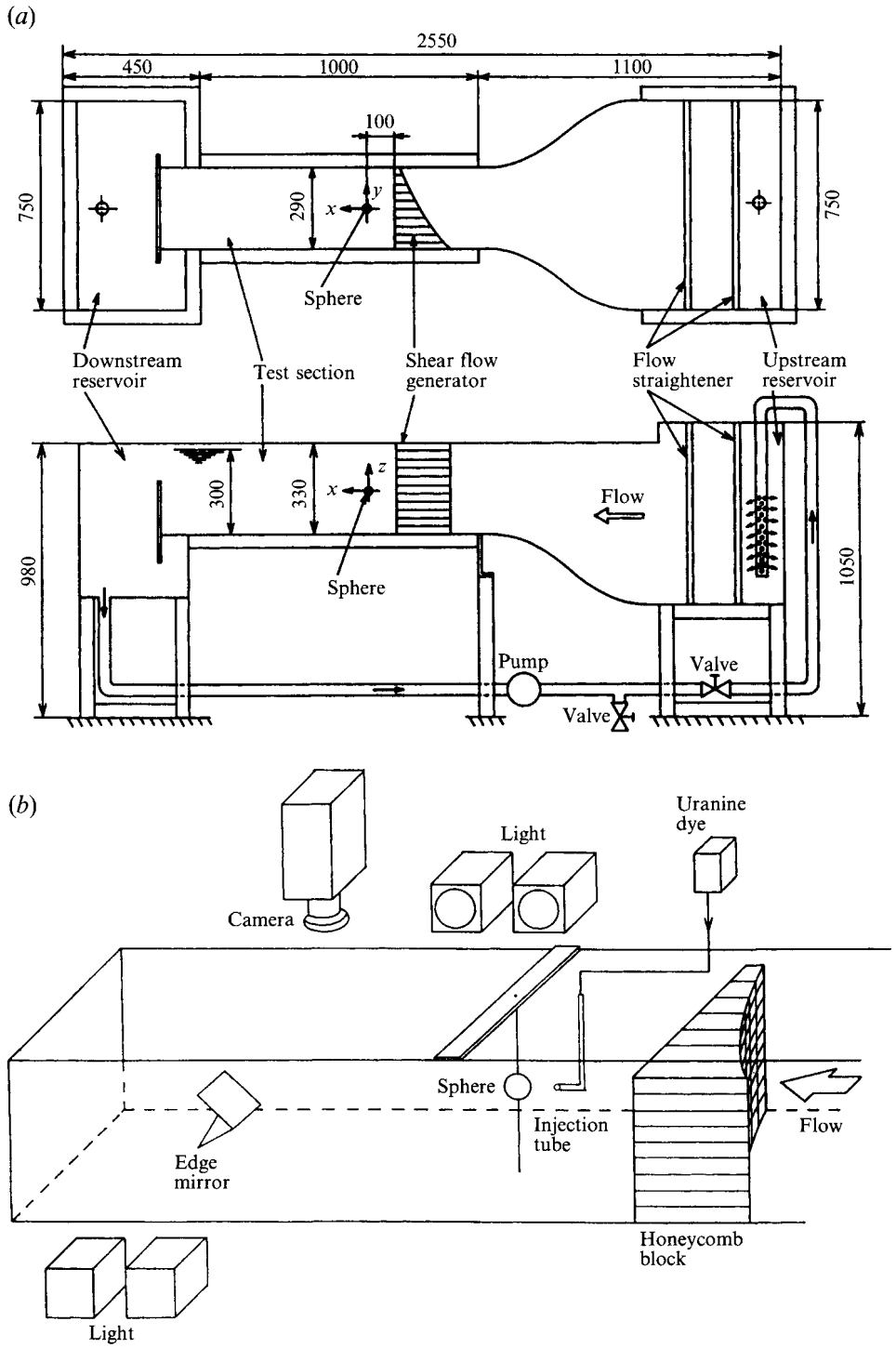


FIGURE 1. Experimental apparatus. (*a*) Schematic diagram of water channel facility (dimensions in mm). (*b*) Schematic diagram of arrangement for honeycomb block, sphere and observation system.

however, no appreciable waves were observed on the free surface during the experiments. The test section of the channel consisted of transparent glass plates 5 mm in thickness to allow flow visualization. Thus, the flow pattern could be observed from the top and sides of the test section. The velocity in the test section was controlled by a valve installed in the return section and varied from 0.8 to 10.3 cm $s^{-1}$ at the sphere centre. Two turbulence-reducing screens, in series, consisting of urethane and wire gauzes were provided in a calming chamber upstream of the test section to break up large disturbances of flow caused by the discharge from the return pipe. Also, in order to obtain a wide range of Reynolds numbers, the kinematic viscosity of the water was varied in the range of 1.146–0.602 $mm^2$ $s^{-1}$ by changing the water temperature from 15 to 45 °C.

Spheres tested were steel balls as used in ball bearings. Thirty-four spheres were employed, with diameters ranging from 3 to 35 mm. All were finished to a high standard and polished so that an assumption of hydraulic smoothness would be justified. Each had a small hole through which was threaded a fine suspension wire 0.1–0.2 mm in diameter which was attached perpendicularly to the floor of the test section shown in figure 1 (*b*). The spheres were fixed at the centre of the test section by the suspension wire. All were positioned 100 mm from the downstream face of a honeycomb block, 150 mm from the floor of the test section and 145 mm from its sidewalls. In many of the reported studies on spheres, the sphere was supported from the rear by a small steel rod. It is somewhat doubtful whether the thin wire used to suspend the spheres in the present study exerts an influence on the boundary layer of the spheres. Taneda (1956) and Pruppacher, Le Clair & Hamielec (1970) have reported that when the Reynolds number of a circular cylinder is smaller than 5.0, the wake almost fails to form, because the separation of the boundary layer occurs near the rear stagnation point. In the present study, since the Reynolds numbers based on the diameter of the suspension wire are smaller than 1.0, the wake formed behind the suspension wire is very small. Also, as mentioned in §4, the Strouhal numbers of a sphere with a suspension wire in a uniform flow almost coincide with those of a sphere supported from the rear by a small steel rod. Thus, it can be considered that the suspension wire scarcely disturbs the boundary layer on the surface of the sphere.

### 2.2. *Measurement procedures*

The distribution of the longitudinal velocity component of the shear flow was obtained by measuring the time of travel of hydrogen bubbles produced by a pulsed voltage from a tungsten wire 10 μm in diameter and 28 cm in length, thereby forming the timelines. The wire was set parallel to the horizontal $y$-axis (see figure 1) and then was arbitrarily moved in the direction of the $x$- and $z$-axes. The visualized timelines were recorded on a video system having a frame rate of 30 frames per second, and then processed by an image-processing method using a computer, so that the velocity distribution of the shear flow was precisely determined.

Wake flow patterns of the sphere in uniform shear flow were visualized by using uranine dye. The uranine dye was injected using a stainless steel tube with a diameter of 1 mm which was positioned 80 mm upstream of the front stagnation point of the sphere. After the uranine dye was injected for the specified period of time, the stainless steel tube was removed from the test section in order to avoid any disturbance generated by it. The visualized wake patterns of the sphere were recorded on a video system with the light-sheet scanning method. The light sheet was swept by driving a cart on which was mounted a slide projector containing a slit cartridge with a width of 2 mm. The cart was reciprocally driven by an induction motor and a crank in the

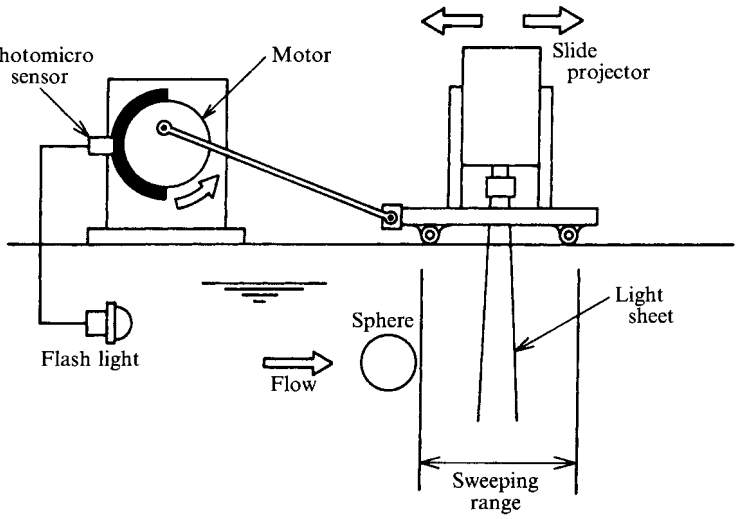


FIGURE 2. Schematic diagram of flow visualization system.

horizontal direction with a stroke of 120 mm, as shown in figure 2. Also, signals from a photomicrosensor attached to the shaft of the induction motor, which repeatedly switches on and off, were recorded by the video system as standard signals for obtaining the sweeping time. Cross-sectional images in the visible range obtained in approximately 1/30 s were reflected by a mirror which was placed at a downstream position and recorded by the video system through a CCD camera. By replaying, on the basis of the signal from the photomicrosensor which provided the information for the sweeping phase, images were digitized frame by frame by a video digitizer and stored in a computer. The time coordinate was then converted into the spatial coordinate to create three-dimensional image data. Since the time interval from frame to frame is 1/30 s, and the sweep period of the light sheet is about 1.40 s, approximately 21 cross-sectional images are taken for one sweep of the light sheet. Also, since the periodicity of the vortex shedding is approximately 8 s, about 11 time-varying three-dimensional images can be obtained for one period of vortex shedding.

The frequency of vortex shedding from the sphere immersed in uniform shear flow was determined on the basis of a power spectrum analysis of the fluctuating velocity detected by a hot-film sensor mounted in the wake behind the sphere. The hot-film sensor was positioned at about three diameters downstream of the rear stagnation point of the sphere. The definition of the coordinate system used in this experiment is presented in figure 1(*a*). The origin of the coordinate system is the centre of the sphere which is located at mid-depth and midway between the sidewalls of the test section. The $x$-axis is in the downstream direction, the $y$-axis is across the channel and the $z$-axis in the depth direction of the test section. A definition sketch of a sphere in uniform shear flow is shown in figure 3. The diameter of the sphere is $d$, the approach velocity at the sphere centre is $U$ and the transverse velocity gradient of the shear flow is denoted by $G$. The longitudinal velocity component will generally be written as $u$.

### 2.3. *Production of uniform shear flow*

The common practice for generating a uniform shear flow is by placing a shear-generating apparatus such as a tapered honeycomb (Kotansky 1966), a grid of parallel rods (Owen & Zienkiewicz 1957), or a pair of closely spaced shaped gauzes (Woo & Cermak 1992) in the flow. In the present study, by applying the method of Kotansky,

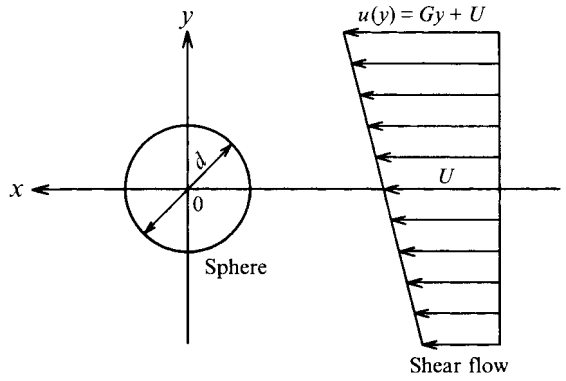


FIGURE 3. Definition sketch of uniform shear flow past a sphere.

a uniform shear flow was produced by a honeycomb block which was installed at the upstream part of the test section, as shown in figure 1(*b*). It was a PVC honeycomb block of hexagonal cells in which the distance between opposite sides (0.1 mm in thickness) was 4 mm, shaped to a first approximation according to the theory of Kotansky. However, a uniform shear flow of sufficient accuracy could not be obtained by a honeycomb block of the first approximation. Next, the honeycomb block was shaped according to the second approximation on the basis of the relationship between the velocity profile of the shear flow generated by the first honeycomb block and its shape. By repeating this procedure two to three times, a honeycomb block which generated a uniform shear flow of sufficient accuracy could be realized.

An example of a velocity profile of a uniform shear flow produced by the present experiment is shown in figure 4, which shows the transverse velocity profile at 100 mm ($x = 0$) from the downstream surface of the honeycomb block at various locations in the $z$-direction. The solid straight line is the best-fit line obtained by applying the least-squares method to the data. The maximum deviation from the mean line is less than $\pm 3\%$. An approximately linear profile was realized in the region $-100 \leqslant y \leqslant 100$ mm. Moreover, it is seen clearly that the velocity distributions at different values of $z$ are similar. The same degree of accuracy was also obtained for all the other shear flows which were used in this study. An example of the fluctuating velocity distribution along the $y$-direction at $x = 0$ mm is also shown in figure 4. The magnitude of turbulence intensity is small, ranging from 0.3% to 0.5%. Accordingly, it can be considered that the turbulence intensity of the approaching flow has little effect on the flow around the sphere. In the present work, five different honeycomb blocks were used to change the velocity gradient of the uniform shear flow. The transverse velocity gradient of the shear flow produced by the honeycomb block changed when both the viscosity of the water, which is dependent on the temperature, and the average velocity in the test section were varied. By changing the temperature and velocity in the test section, the velocity gradient of the shear flow $G$ could be varied in the range of 0.04 to 0.55 $s^{-1}$. Honeycomb generators of shear flow will produce less turbulence than grid of parallel circular rods arranged with varying spacing along the plane of the grid (Owen & Zienkiewicz), and the turbulence intensities are at the same level as those by the method of Woo & Cermak, in which a pair of closely spaced curved gauzes with the upstream gauze of varying porosity and the downstream gauze of uniform porosity was used.

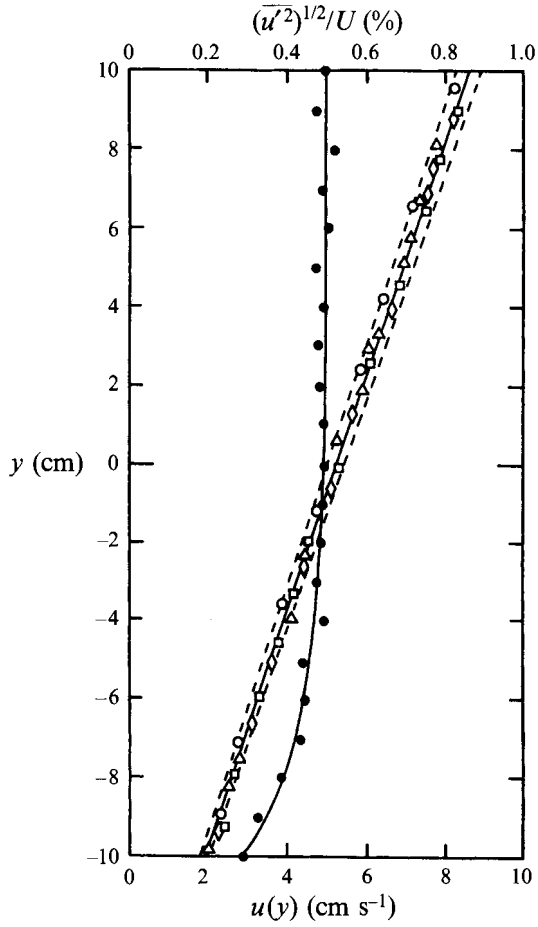


FIGURE 4. An example of time-mean and fluctuating velocity of uniform shear flow at the position where test sphere is set up ($x = 0$) at various locations in the $z$-direction: ——, best-fit straight line for averaged slope $G = 0.345$ S$^{-1}$; -----, deviation of $\pm 3\%$ from best-fit lit line; ○, $z = +100$ mm; △, $z = +50$ mm; □, $z = -50$ mm; ◇, $z = -100$ mm; —●—, distribution of fluctuating velocity along the $y$-direction.

## 3. Parameters to be included

There are six parameters which govern the vortex shedding frequency of a sphere in a uniform shear flow: the diameter of the sphere $d$, the approach velocity at the sphere centre $U$, the transverse velocity gradient of the shear flow $G$, the kinematic viscosity of the fluid $\nu$, the projected area of the sphere $S$ and the cross-sectional area of the test section $C$. Therefore, the functional relationship for the frequency $f_c$ of vortex shedding from a sphere in uniform shear flow can be written as

$$f_c = \phi(d, U, G, \nu, S, C). \tag{1}$$

By dimensional analysis, the Strouhal number based on the vortex shedding frequency $f_c$ of the sphere can be written as

$$St = f_c d/U = \phi(Ud/\nu, Gd/U, S/C). \tag{2}$$

Since $S$ is the projected area of the sphere, $S/C$ is the blockage ratio for the three-

dimensional body (Modi & Akutsu 1984). By introducing the Reynolds number $Re$ and the shear parameter $K$, which are defined by

$$Re = Ud/\nu, \quad K = Gd/U, \tag{3}$$

the functional relationship (2) can be expressed as

$$St = \phi(Re, K, S/C). \tag{4}$$

We now discuss the effect of the blockage ratio $S/C$ included in (4). Modi & Akutsu (1984) have reported on the blockage effects on spheres in the Reynolds number range of 30–2000. Many detailed plots of pressure distributions, total drag and skin friction, the separation point of the boundary layer and the wake configuration of the spheres for the various blockage ratios are given in their paper. They have concluded that the blockage effects are essentially negligible up to around 11% blockage. The maximum blockage ratio $S/C$ in the present study was 1.1%, which is very small compared with the criterion set by Modi & Akutsu. Thus, since the vortex shedding frequency is closely associated with the surface pressure, separation point and wake configuration of the sphere, it can be concluded that the Strouhal numbers obtained by the present study are practically uninfluenced by the wall confinement effects. As a result, the functional relationship (4) can finally be put in the following form:

$$St = \phi(Re, K). \tag{5}$$

Consequently, one of the main purposes of the present study is to clarify the functional relationship (5) by varying the above two non-dimensional parameters. However, it was difficult to perform experiments in which $K$ was constant for a wide range of Reynolds numbers because the Reynolds number must be varied while maintaining a constant value of $d/U$ even if the velocity gradient $G$ remains constant. Accordingly, a relationship among $Re$, $K$ and $St$ was inferred in the same manner as employed by Kiya, Tamura & Arie (1980), who have investigated the Strouhal number of two-dimensional circular cylinders in a uniform shear flow. Since the shear parameter and the Reynolds number are proportional to the sphere diameter $d$, if a combination of $G$, $U$ and $\nu$ is given, the measurement of the vortex shedding frequency as a function of the diameter yields a relation among $Re$, $K$ and $St$. From the relation among these variables, one can obtain the Strouhal number for a particular value of $K$ by a linear interpolation.

## 4. Results and discussion

### 4.1. *Structure of the hairpin vortex loop*

Investigation of the structure of the hairpin vortex loop shed from a sphere in uniform shear flow was carried out at the Reynolds number where the vortex loops are detached in the regular mode. The uranine dye-visualization technique was extensively employed to study the structure of the hairpin-shaped vortex loops and their evolution. Figure 5 shows side-, top- and end-view dye visualizations of the vortex loop for $Re = 355$ and $K = 0.158$. These photographs show the successive wake configurations when the time taken to detach one vortex loop is divided equally into five parts. As is obvious from the side-view pictures, a separated shear layer begins rolling up cylindrically at the rear of the sphere immediately after a previous hairpin-shaped vortex loop is detached. Since the rolling up of the shear layer on the high-velocity side is stronger than that on the low-velocity side, the vorticity entraining in the vortex formation region from the high-velocity side is larger than that from the low-velocity side. Thus, the growth of

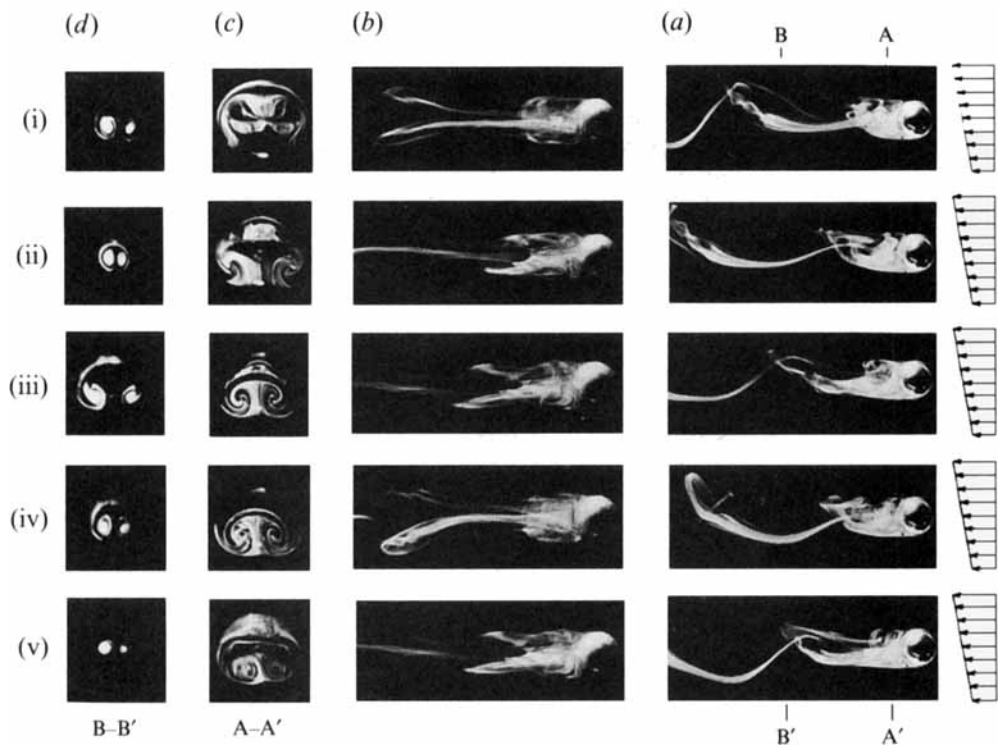


FIGURE 5. Photographs of the shedding pattern of hairpin-shaped vortex loops over one period $T$ for $Re = 355$ and $K = 0.158$: (i) $T = 1/5$; (ii) $T = 2/5$; (iii) $T = 3/5$; (iv) $T = 4/5$; (v) $T = 5/5$. (*a*) Side-view, (*b*) top-view, (*c*) end-view (cross-section A–A′), (*d*) end-view (cross-section B–B′).

vortex that forms on the high-velocity side is faster than that on the low-velocity side, and hence a vortex formed on the high-velocity side continues to grow while taking in the vorticity from the surrounding shear layer which is rolling up cylindrically. The growing vortex on the high-velocity side is cut off by the hollow which is formed by the development of instabilities (presumably Tollmien–Schlichting instabilities) generated on a part of the shear layer between the nascent vortex and the spiral vortex, and then is detached as a hairpin-shaped vortex loop. Also, from the top-view visualization it can be observed that the legs and head of the vortex loop are detached from the vortex formation region as the hairpin undergoes a stretching process. Figures 5(*c*) and 5(*d*) are the end-view visualization of the vortex loop. A front-silvered wedge mirror was located far downstream of the sphere location to avoid upstream effects of the mirror on hairpin vortex generation. The apex angle of the mirror was optimized at 45°, which was found to minimize blockage effects while providing a sufficient reflection angle. As is clearly seen from photograph of cross-section A–A′, the shear layer which rolls up symmetrically at the bottom of the low-velocity side is taken into the vortex region on the high-velocity side while pushing up the two vortex tubes which are the roots of the previous vortex loop. Cross-section B–B′ shows a section of the detached vortex loop. This figure clearly demonstrates the rotation of the legs of the vortex loop formed on the high-velocity side, and then these clearly change in size with time.

The above description is based on the configuration of a laminar wake containing hairpin-shaped vortex loops. However, when the wake behind the sphere becomes turbulent, the structure of vortices is extremely obscure as shown in figure 7(*b*), and is

(a)

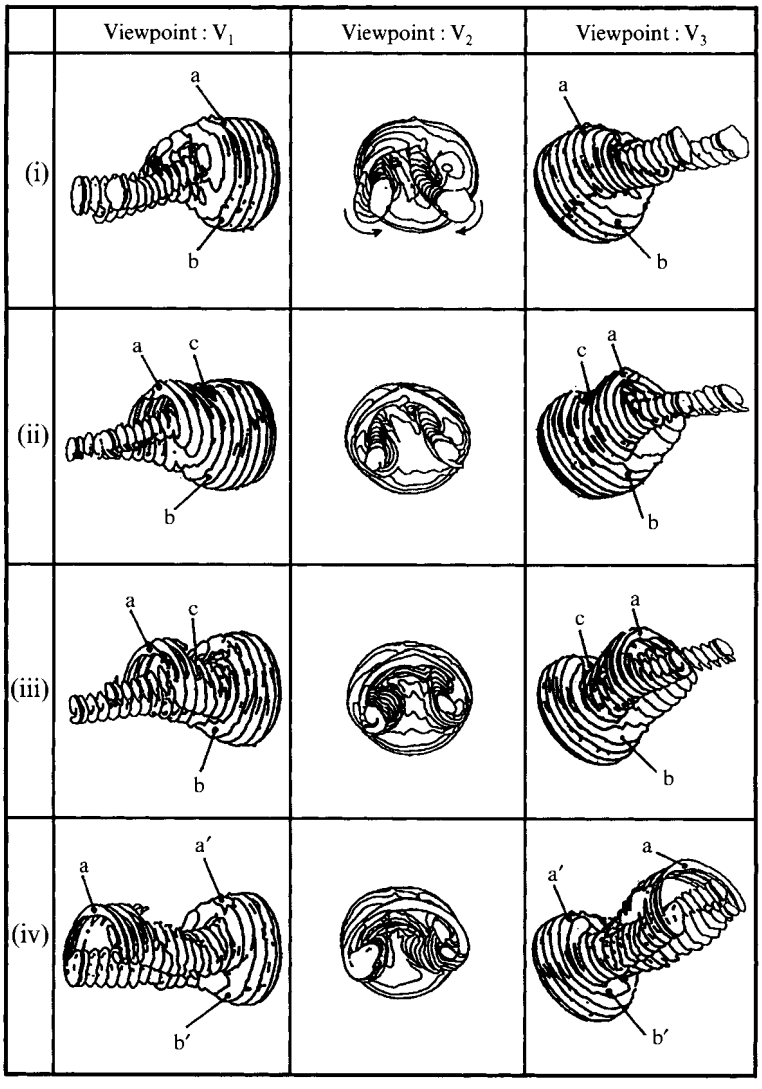


(b)

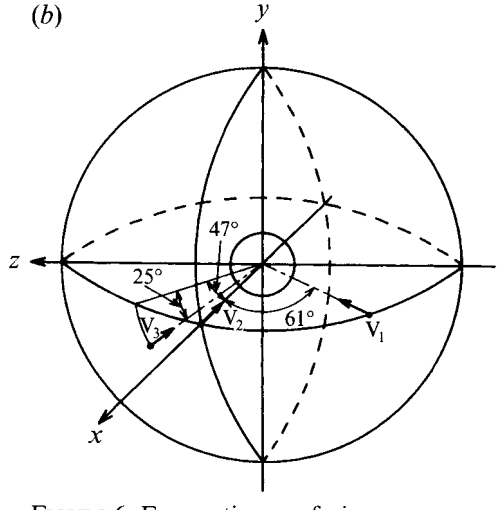


FIGURE 6. For caption see facing page.

most difficult to describe in detail. Perry & Watmuff (1981) investigated the structure of the turbulent wake behind an axisymmetric blunt body using a flying hot-wire apparatus and clarified that the geometry of the phase-averaged vector field displays the same general features as a hairpin-shaped vortex loop at low Reynolds numbers (unsteady laminar wake). Also, Perry & Lim (1978) reported that the large-scale eddy structures behind blunt three-dimensional bodies such as spheres are substantially the same. Therefore, the turbulent wake of a sphere is considered to have essentially the same general structure as the vortex loop system of the laminar wake, as shown in figure 5(*a*). Furthermore, Sakamoto & Haniu (1990) have already elucidated the formation mechanism of a vortex detached from the sphere in uniform flow. Its formation mechanism and configuration are exactly the same as in the case of uniform shear flow except for the detachment point of the vortex loops, i.e. the detachment point of the vortex loops is always fixed on the high-velocity side in the case of uniform shear flow, while it is not fixed in the case of uniform flow.

In order to understand the instability of the vortex loops formed behind a sphere in a uniform shear flow, a good knowledge of the wake of the sphere in uniform flow is necessary. In the Reynolds number range studied for the uniform flow, three instability modes are excited: one, an axisymmetric pulsation of the recirculating zone with vortex shedding; two, an axisymmetric vortex shedding associated with the shear at the periphery of the recirculating zone; and three, a spiral mode related to a rotation of the separation line. When the Reynolds number exceeds 300, the first instability is excited and vortex shedding occurs (Taneda 1956). Vortex loops forming a series of interlocking loops are emitted regularly behind the sphere. When the Reynolds number exceeds 800, the second instability is excited and the two modes are simultaneously present but are unlocked (Kim & Durbin 1988; Sakamoto & Haniu 1990). The third instability is associated with the rotation of the separation line on the sphere, resulting in a spiral mode. These instability modes do not substantially change the wake structure of the vortex loop system, but they do affect the vortex shedding frequency mode. These loop-like structures in wakes behind the sphere were also encountered in the wakes behind axisymmetric bodies and coflowing jets and wakes (Perry & Lim 1978). They resemble a daisy chain of interlocking loops which is similar to the ladder-like structure sketched by Achenbach (1974). Accordingly, since these vortex loops shed behind the sphere form a series of interlocking loops, the hairpin vortices flow out, maintaining a stable condition regardless of the single row of vortices.

### 4.2. *Formation process of hairpin-shaped vortex loops*

The formation process of the hairpin-shaped vortex loops shed from a sphere immersed in a uniform shear flow was examined on the basis of the image-processing methods for $Re = 375$ and $K = 0.1$, at a Reynolds number at which the configuration of the vortex loops is clearly conserved far downstream without being diffused. Figure 6(*a*) shows the successive formation process of a detached vortex loop over one cycle of vortex shedding. These results represent the three-dimensional visualization images observed from viewpoints $V_1$, $V_2$, $V_3$, as shown in figure 6(*b*). At the first stage, as shown in figure 6(*a*)(i), ring-shaped separation bubbles begin to grow so as to cover the rear part of the sphere. In particular, it is worth noting that the growth of separation

FIGURE 6. Formation process of a hairpin-shaped vortex loop represented schematically using the image-processing method, over one period for $Re = 375$ and $K = 0.1$. (*a*) Time variation of quasi-instantaneous three-dimensional images: (i) $T = 1/4$; (ii) $T = 2/4$; (iii) $T = 3/4$; (iv) $T = 4/4$. (*b*) Coordinate system for viewpoints $V_1$, $V_2$, $V_3$.

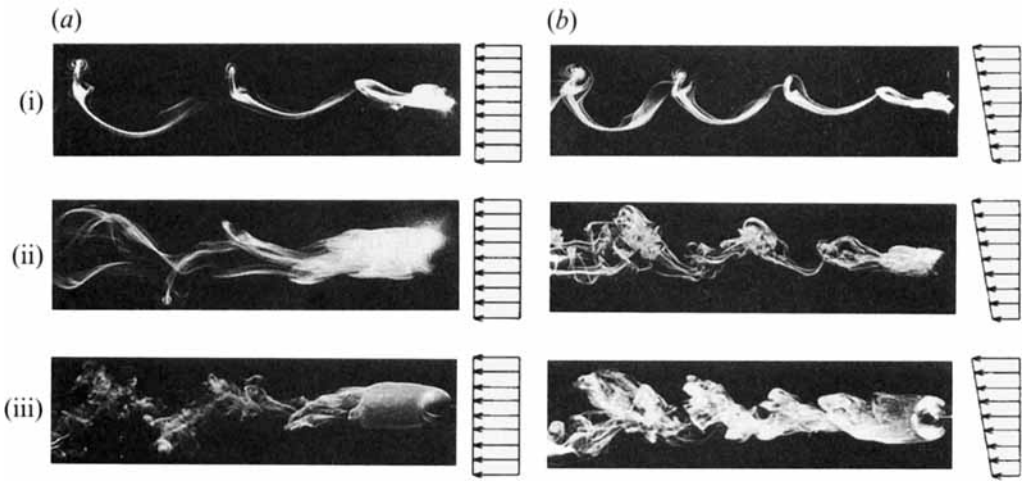


FIGURE 7. Side-view visualization of hairpin vortices. (*a*) Uniform flow: (i) Region I ($Re = 350$); (ii) Region II ($Re = 650$); (iii) Region III ($Re = 1350$). (*b*) Uniform shear flow: (i) Region I ($Re = 355$, $K = 0.071$); (ii) Region II ($Re = 780$, $K = 0.158$); (iii) Region III ($Re = 1444$, $K = 0.167$).

bubbles on the high-velocity side (labelled a) is faster than that on the low-velocity side (labelled b). At the second stage, as shown in figure 6(*a*)(ii), the separation bubbles on the high-velocity side grow in such a manner as to encircle two vortex tubes of a previous vortex. However, the growth of bubbles on the low-velocity side (labelled b) is slow and the ring shapes of separation bubbles still remain. Also, a hollow which is formed by the development of instabilities is generated on a part of the shear layer between the nascent vortex and the spiral vortex as indicated by label c. At the third stage, as shown in figure 6(*a*)(iii), the growing vortex on the high-velocity side is cut off by the hollow, and then is detached as a hairpin-shaped vortex loop. However, the separation bubbles (labelled b) on the low-velocity side shrink without growing into vortex loops because the vorticity entraining from the low-velocity side is absorbed by the two vortex tubes created on the high-velocity side. At the last stage, as shown in figure 6(*a*)(iv), the separation bubbles indicated by labels a′ and b′ grow again to form the hairpin-shaped vortex loops. As is clearly seen from the above-mentioned results, when the sphere is placed in a uniform shear flow, the growth of separation bubbles into a vortex loop on the high-velocity side is much faster than that on the low-velocity side. As a result, since the separation bubbles generated on the low-velocity side are absorbed by the vortex loops formed on the high-velocity side before they can grow into a vortex loop, the hairpin-shaped vortices are always detached from the high-velocity side.

Figure 7 shows pictures of detached vortex loops from spheres placed in uniform flow and shear flow for different Reynolds numbers. When $Re$ exceeds 300, the detached vortex loops from the sphere in the uniform flow begin to be shed with regularity in strength and frequency. Also, as shown in figure 7(*a*)(i), once the detachment point of the vortex loops is fixed, it does not change for a long time. However, as shown in figure 7(*b*)(i), the vortex loops are always detached from the high-velocity side in the uniform shear flow. When $Re$ exceeds 420 in uniform flow, the vortex loops begin to be shed irregularly in directions that oscillate intermittently from right to left. Furthermore, the vortex loops flow out with a twisted posture, as shown in figure 7(*a*)(ii), because the magnitudes of circulation of the two vortex tubes whose directions of rotation are opposite to each other are different. In the case of uniform

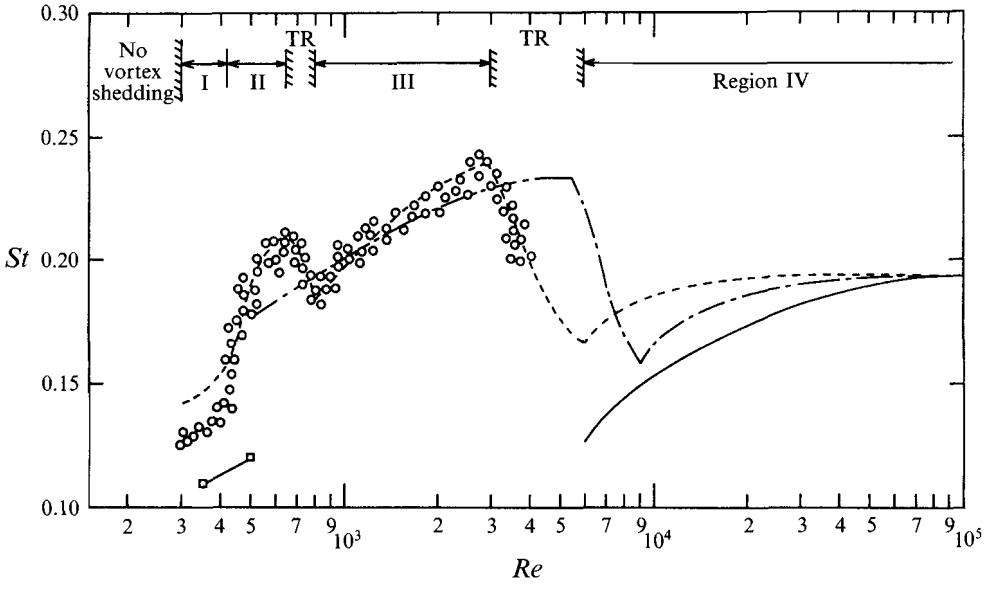


FIGURE 8. Strouhal number versus Reynolds number for uniform flow: ○, present data ($K = 0$); -----, Sakamoto & Haniu (1990); —·—, Kim & Durbin (1988); ———, Achenbach (1974); □—□, Magarvey & Bishop (1961).

shear flow, the twisting of the entire loops is small compared with that in uniform flow, as shown in figure 7(*b*)(ii), since the detachment point is always fixed on the high-velocity side. When *Re* exceeds 800 in uniform flow, the separation bubbles located at a symmetrical position to that where vortex loops are detached begin to form loops independently. As a result, vortex loops are alternately detached from mutually symmetrical positions, as shown in figure 7(*a*)(iii). However, in uniform shear flow, the alternating detachment of vortex loops does not take place as shown in figure 7(*b*)(iii), since the vortex loops are formed on the high-velocity side only.

### 4.3. *Strouhal number*

In order to demonstrate the reliability of the present measurements, the vortex shedding frequency of a sphere in uniform flow was examined. Figure 8 shows the Strouhal number plotted against the Reynolds number for spheres in uniform flow together with the data of Kim & Durbin (1988), Sakamoto & Haniu (1990), Achenbach (1974) and Magarvey & Bishop (1961) for comparison. The results of Sakamoto & Haniu were obtained in a wind tunnel, and the present data are almost the same except for those for Reynolds numbers lower than 400. In the wind tunnel test performed by Sakamoto & Haniu (1990), the free-stream velocity at Reynolds numbers below 400 was estimated by using Roshko's (1956) formula based on the vortex shedding frequency from a two-dimensional circular cylinder. However, since the first extensive measurements of vortex shedding frequencies by Roshko, there has been remarkably little agreement among the many published curves of Strouhal number versus Reynolds numbers for the laminar shedding region, which differ by almost 20% (Williamson 1989). Thus, this discrepancy between the two results at Reynolds numbers below 400 may be caused by an error involving the values of free-stream velocity estimated by using Roshko's formula in the wind tunnel test. Also, the values of the Strouhal number measured by Kim & Durbin are similar to those obtained in

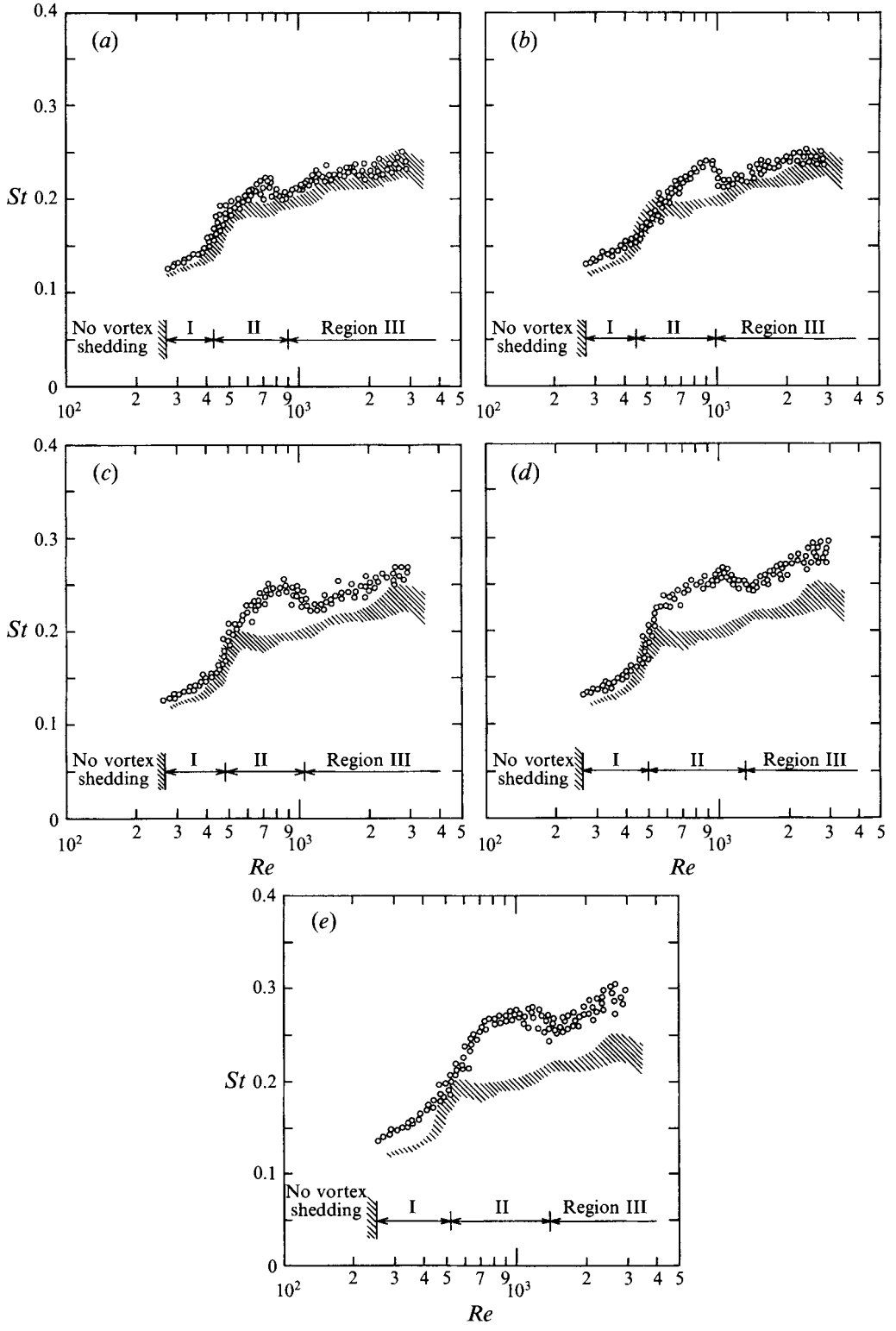


FIGURE 9. Strouhal number versus Reynolds number for different values of the shear parameter: ○, present data for shear flow; ▨, present data for uniform flow. (*a*) $K = 0.05$, (*b*) $K = 0.10$, (*c*) $K = 0.15$, (*d*) $K = 0.20$, (*e*) $K = 0.25$.

the present study; however, the features of the change in the Strouhal number with Reynolds number show considerable differences. For example, the Reynolds number at which the Strouhal number decreases rapidly is about $5.5 \times 10^3$ in the results of Kim & Durbin, but it is about $3 \times 10^3$ in the present study. Kim & Durbin measured the Strouhal number of a sphere in periodically excited flow which was provided by a loudspeaker, thus the discrepancy may be caused by the difference between a steady flow and an excited flow in which the vortex shedding frequency is locked in. Achenbach reported that for Reynolds numbers smaller than $6 \times 10^3$, periodic vortex shedding did not occur, but from $Re = 6 \times 10^3$ to $3 \times 10^5$ strong periodic fluctuations in the wake flow were observed. In the wind tunnel test performed by the present authors, vortex shedding with pseudoregularity also began to occur when the Reynolds number exceeded $6 \times 10^3$. It is possible that the shear layer separated from the surface of the sphere changed from laminar to turbulent flow. Furthermore, it was demonstrated that the change in Strouhal number with Reynolds number could be classified into four regions, as shown in figure 8, based on the difference in wake configuration. Region I is the range between $Re = 300$ and 420 where the hairpin-shaped vortex loops are periodically shed in what is called a regular mode with regularity in strength and frequency. Region II includes the transitional region and is the range between $Re = 420$ and 800 where the vortex loops are shed in the irregular mode. Region III is the range between $Re = 800$ and 3000 where the vortex loops change from laminar to turbulent vortices. Also, in this region, the high-frequency mode of the Strouhal number which is associated with small-scale instability of the separating shear layer begins to be periodically generated together with the low-frequency mode. When the Reynolds number exceeds about $3 \times 10^3$ (transitional region), the shear layer separating from the surface of the sphere begins to change from laminar to turbulent, and then it becomes completely turbulent at a Reynolds number of $6 \times 10^3$. Also, periodic vortex shedding with the low mode frequency continues as far as the critical Reynolds number of $3.7 \times 10^5$ (Region IV).

Figure 9 shows the Strouhal number as a function of the Reynolds number for several values of the shear parameter in the range $K = 0.05$–$0.25$. For low values of $K$ the Strouhal number for shear flow differs little from that for uniform flow, whereas for the larger shear parameters ($K > 0.1$) it is generally higher. The Strouhal number can also be classified into three regions for each value of $K$ in the range up to $Re = 3 \times 10^3$, which was done in the present study. The following is an explanation of the relationship between the change in the Strouhal number and the configuration of the wake in each region, including a comparison with uniform flow.

*Region I.* Figure 10 shows the waveform and power spectrum of the fluctuating velocity which was detected by the hot-film sensor set in the wake behind the sphere. In Region I, the power spectrum distribution with a line spectral peak and the amplitudes of the waveform of the fluctuating velocity as shown in figure 10(*b*) suggest that the hairpin-shaped vortex loops are periodically shed in what is called a regular mode with regularity in strength and frequency. As already mentioned, the hairpin vortices shed from the high-velocity side of the sphere flow out, forming a single row of vortices. Roshko (1976) demonstrated that there is no spectral peak in the frequency spectrum of a single row of vortices formed in turbulent shear flow. However, since there is a prevailing frequency, as shown in figure 10(*b*), the hairpin vortices are shed with this prominent frequency regardless of the single row of vortices. The present authors (1990) have already reported that hairpin-shaped vortex loops with a regular mode continue to be seen up to $Re = 420$ for a sphere immersed in a uniform flow. Magarvey & Bishop (1961) also observed that this phenomenon continues until a

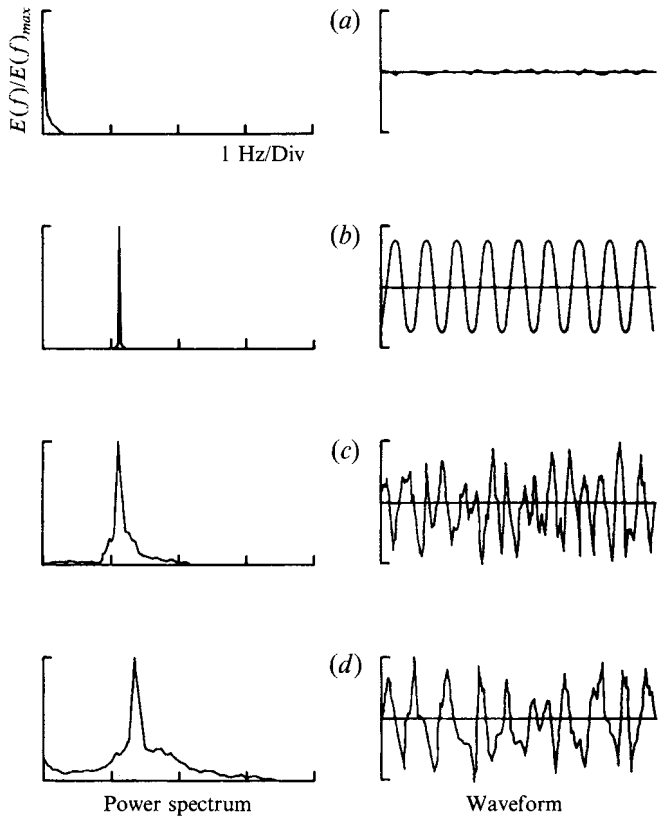


FIGURE 10. Waveform and power spectrum of fluctuating velocity. (*a*) No vortex region ($Re = 220$, $K = 0.087$), (*b*) Region I ($Re = 355$, $K = 0.071$), (*c*) Region II ($Re = 780$, $K = 0.158$), (*d*) Region III ($Re = 1444$, $K = 0.167$).

Reynolds number of about 410 is reached. The noteworthy aspect of the vortex shedding pattern in uniform shear flow is that the upper limit of the Reynolds number where the hairpin-shaped vortex loops are shed in the regular mode increases as the shear parameter is increased. For example, it extends up to $Re = 480$ for $K = 0.15$ and to $Re = 520$ for $K = 0.25$. It is well known that the vortices shed from a bluff body are formed by the concentration of vorticity entraining into the vortex formation region. When the vorticity entraining into the vortex formation region is very regularly supplied, stored and emitted, successive vortices are of the same strength and frequency, i.e. the shedding pattern of the vortices is always in the regular mode. When the Reynolds number exceeds 420 for a sphere immersed in uniform flow, the diffusion of the vorticity entraining into the vortex formation region is a result of the irregular change of the detachment point of the vortex loops. Thus the hairpin-shaped vortex loops begin to be generated with irregularity because the rates of vorticity concentration differ from one another. However, in uniform shear flow diffusion of the vorticity resulting from the change of the detachment point of the vortices does not occur because the detachment point is always fixed on the high-velocity side. Accordingly, the balance between the supply and emission of vorticity within the vortex formation region is retained up to a higher Reynolds number than for uniform flow and so vortices are periodically shed with regularity in strength and frequency. Also, there is

no remarkable increase of Strouhal number with an increase in the shear parameter $K$ in this region.

*Region II.* In this region, which includes the transition from Region I to II and from II to III, the waveform of the fluctuating velocity based on the shedding of the hairpin vortices becomes irregular, as shown in figure 10(*c*). The spectral peak in the power spectrum distribution also shows a band spectrum. Thus the shedding pattern of the vortices is irregular. Also, the upper limit of the Reynolds number in this region increases with the increase of the shear parameter $K$. For example, it extends up to $Re = 1050$ for $K = 0.15$ and $Re = 1400$ for $K = 0.25$, compared to $Re = 800$ for uniform flow. The Strouhal number is larger than in uniform flow and increases with an increase of the shear parameter $K$. For uniform flow, in this region the detachment point of hairpin-shaped vortex loops changes irregularly, and they flow out with oscillation from left to right. However, for uniform shear flow, their detachment point is fixed on the high-velocity side, and scarcely any oscillations of the detached vortex loops occurs, as seen in figure 7(*b*)(ii). In general, the vortices are shed in a state of equilibrium between the supply and emission of vorticity in the vortex formation region. Accordingly, when the vorticity entraining in the vortex formation region increases, the formation of vortices is promoted so that the vortex shedding frequency is increased. Therefore, the Strouhal number becomes larger than in uniform flow since the vortex loops are formed in a shorter time because of both the increase of entrainment from the high-velocity side and no vorticity consumption in the vortex formation region caused by the change of the detachment point.

*Region III.* For uniform flow in this region, the cylindrical vortex sheet separated from the sphere surface shows pulsation, and small vortex loops begin to be periodically shed from the vortex formation region in accordance with the pulsation (known as high-mode vortex shedding). Some of the small vortex loops diffuse rapidly, and others move downstream, intricately intertwining with the large-scale vortex loops (known as low-mode vortex shedding). For uniform shear flow, these features are qualitatively similar, and then the lower- and higher-frequency modes of the Strouhal number coexist (only the Strouhal number in the low-frequency mode was measured in the present study). The detached large-scale vortices, which may be of the same structure as a hairpin-shaped vortex loop, flow out from the high-velocity side without rotation at random, as indicated in figure 7(*b*)(iii), while in uniform flow, these move away from the sphere, rotating at random about an axis parallel to the flow through the centre of the sphere. Also, for $K < 0.1$, there is little change in the Strouhal number with the shear parameter. An unmistakable effect of the shear parameter becomes clear only for $K > 0.1$, in which the Strouhal number increases with an increase of the shear parameter. Furthermore, as is shown in figure 8, the Strouhal number changes rapidly when the Reynolds number exceeds about $3 \times 10^3$ in uniform flow because the shear layer which separates from the sphere surface begins to change from laminar to turbulent flow, i.e. a transition from Region III to IV occurs when the Reynolds number exceeds about $3 \times 10^3$. In uniform shear flow, a change in the critical Reynolds number from Region III to IV is not certain because measurements were done only up to $Re = 3 \times 10^3$ in the present study. However, it is presumed that the upper limit of the Reynolds number indicated for Region III also becomes larger with the increase of the shear parameter, since these become larger in both Regions I and II.

### 4.4. *The critical Reynolds number at which vortex shedding occurs*

Kiya *et al.* (1980) have experimentally investigated the frequency of vortex shedding from a two-dimensional circular cylinder immersed in a uniform shear flow by

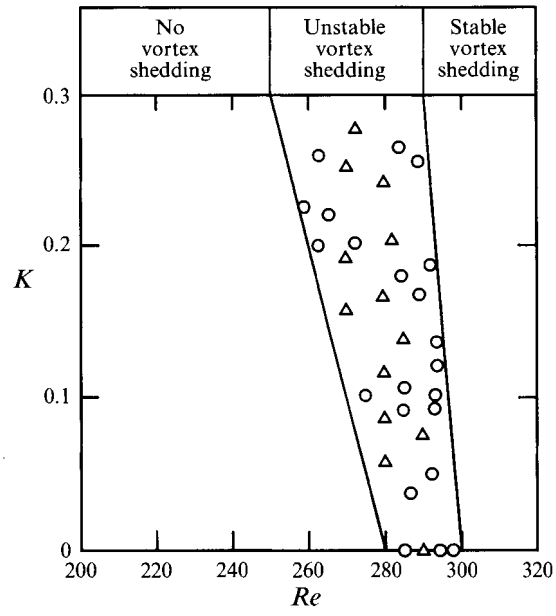


FIGURE 11. Relationship between critical Reynolds number for vortex shedding and shear parameter: △, a pair of undulating threads; ○, a loop-shaped vortex; ——, eye-fit boundary line.

changing the Reynolds number and shear parameter. They have elucidated that the critical Reynolds number at which the vortex shedding occurred was higher than that in the case of uniform flow and increased approximately linearly with the increase of the shear parameter; for example, the vortex shedding which began at about $Re = 50$ in uniform flow occurred at $Re = 70$ for $K = 0.1$, 110 for $K = 0.15$, 160 for $K = 0.2$ and 220 for $K = 0.25$.

Figure 11 shows the relationship between the Reynolds number at which the hairpin vortices from a sphere in uniform shear flow begin to be shed and the shear parameter. This Reynolds number will henceforth be called the critical Reynolds number. As seen in figure 11, the critical Reynolds number decreases with the increase of the shear parameter, contrary to the behaviour of the Kármán vortex street for a two-dimensional cylinder. This may be caused by the difference in vortex formation process. The formation of a Kármán vortex street is dependent on the interaction of two separated shear layers rolling up into the vortex formation region; the growing vortex on one side continues to be fed by vorticity from the shear layer until the vortex becomes strong enough to be drawn by the vortex growing on the other side across the wake. Thus the vortex formation is strongly dependent on the balance between entrainment of fluid bearing vorticity from two shear layers and the concentration and dissipation of vorticity in the vortex formation. Accordingly, the Kármán vortex street formed behind a circular cylinder in uniform shear flow is gradually restrained compared with that in uniform flow as the balance of entrainment of fluid bearing vorticity from the two shear layers is lost. On the other hand, the hairpin vortices formed behind a sphere in uniform shear flow are always formed on the high-velocity side, and their growth is promoted since the entrainment from the separated shear layer rolling up from the high-velocity side increases with increase of the shear parameter. As a result, vortex shedding from the sphere in uniform shear flow begins at a smaller Reynolds number than in uniform flow.

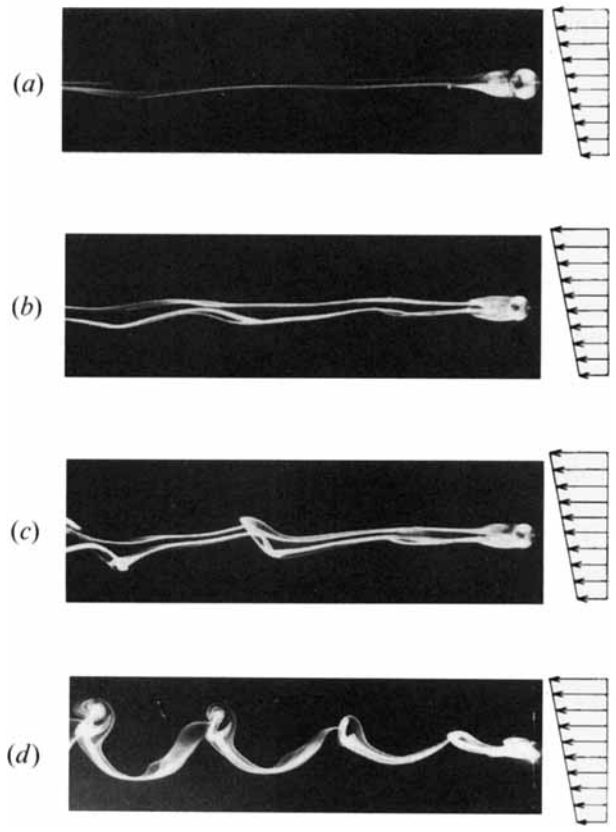


FIGURE 12. Photographs of wake flow patterns in the neighbourhood of the critical Reynolds number. (*a*) A pair of rectilinear threads ($Re = 228$, $K = 0.077$), (*b*) a pair of undulated threads ($Re = 284$, $K = 0.086$), (*c*) unstable vortex loops ($Re = 284$, $K = 0.086$), (*d*) stable vortex loops ($Re = 355$, $K = 0.071$).

Kiya *et al.* (1980) have also shown that two wake patterns appear intermittently in the forms of an incipient vortex street (Morkovin 1964) and a Kármán vortex street in a transitional region where there begins to be a change from a wavy wake to a Kármán vortex street. In the case of a sphere in uniform shear flow, the two wake patterns of a wavy wake and a hairpin-shaped vortex loop appear alternately with irregularity until the Reynolds number at which the hairpin-shaped vortex loop begins to be shed in a stable condition is reached, i.e. a pair of undulating threads and a vortex loop coexist at the same Reynolds number of $Re = 284$, as shown in figure 12. The unstable vortex shedding region differs slightly in accordance with the shear parameter as shown in figure 11. Also, Magarvey & Bishop (1961) have investigated the formation and structure of nearly spherical liquid drop wakes corresponding to a range of Reynolds numbers from 0 to 2500. For Reynolds numbers less than 410, they determined that the following trailing shapes appear with increasing Reynolds number:

Stage I, a single rectilinear thread for $Re < 210$;

Stage II, a pair of rectilinear threads for $210 < Re < 270$;

Stage III, a pair of undulated threads for $270 < Re < 290$;

Stage IV, a procession of vortex loops for $290 < Re < 410$.

The wake configuration of a sphere immersed in uniform flow ($K = 0$) obtained in the present study is almost the same as that described by Magarvey & Bishop except for

slight difference in the Reynolds number range. On the other hand, Achenbach (1974) has reported that a pair of undulating threads turns into a hairpin-shaped vortex when a Reynolds number of about 400 is reached. However, the range of Reynolds numbers of $300 < Re < 420$ at which the hairpin vortices are shed with regularity in the present study corresponds well to the classification of Magarvey & Bishop.

## 5. Concluding remarks

The vortex shedding frequency and the wake structure of a sphere immersed in uniform shear flows were examined. The Reynolds number, defined in terms of the sphere diameter and approach velocity at its centre, ranged from 200 to 3000. The lower value was chosen so as to include the Reynolds number at which vortex shedding from a sphere in uniform flow occurs. Also, the shear parameter, which is the transverse velocity gradient of the shear flow, non-dimensionalized by the approach velocity and sphere diameter, was varied from 0 to 0.25. The main results for a uniform shear flow can be summarized as follows.

(i) The critical Reynolds number above which vortex shedding from the sphere occurred was lower than that in uniform flow and decreased approximately linearly with the increase of the shear parameter.

(ii) The Strouhal number of vortex shedding from the sphere was larger than that in uniform flow and increased with the increase of the shear parameter because the entrainment of fluid bearing vorticity from the shear layer on the high-velocity side increased.

(iii) The vortex generated on the high-velocity side of the vortex formation region gradually grew, taking in vorticity from the surrounding shear layer, and was always detached in the form of a hairpin-shaped vortex loop from the high-velocity side, whereas the detachment point of a vortex loop in uniform flow changed irregularly.

(iv) Two wake patterns, in the form of a pair of undulating threads and a hairpin-shaped vortex loop, appeared alternately with irregularity in the Reynolds number range $Re = 260$–$300$, with Reynolds number differing slightly for each value of the shear parameter, immediately before the $Re$ at which the vortex loops began to be shed stably.

(v) The variation of the Strouhal number with the Reynolds number up to $Re = 3000$ was classified into three regions, and the relationship between the Strouhal number and the wake configuration in each region was determined. It was found that the wake configuration in each region does not differ substantially from that for the uniform flow.

The authors express their sincere thanks to Mr Y. Obata, Kitami Institute of Technology, for his assistance in the construction of the experimental apparatus. Thanks are also due to Mr M. Sakakibara and Mr S. Hirata, graduate students at the authors' Laboratory of Fluid Mechanics in the Department of Mechanical Engineering, for their assistance in the analysis of the experimental data.

## REFERENCES

ACHENBACH, E. 1974 Vortex shedding from spheres. *J. Fluid Mech.* **62**, 209–221.

AUTON, T. R. 1987 The lift force on a spherical body in a rotational flow. *J. Fluid Mech.* **183**, 199–218.

BRETHERTON, F. P. 1962 The motion of rigid particles in a shear flow at low Reynolds number. *J. Fluid Mech.* **14**, 284–304.

COMETTA, C. 1957 An investigation of the unsteady flow pattern in the wake of cylinders and spheres using a hot wire probe. *Div. Engng, Brown University, Tech. Rep.* WT-21.

DANDY, D. S. & DWYER, A. H. 1990 A sphere in shear flow at finite Reynolds number: effect of shear on particle lift, drag, and heat transfer. *J. Fluid Mech.* **216**, 381–410.

HALL, G. R. 1967 Interaction of the wake from bluff bodies with an initially laminar boundary layer. *AIAAJ.* **5**, 1386–1392.

KIM, K. J. & DURBIN, P. A. 1988 Observation of the frequencies in a sphere wake and drag increase by acoustic excitation. *Phys. Fluids* **31**, 3260–3265.

KIYA, M., TAMURA, H. & ARIE, M. 1980 Vortex shedding from a circular cylinder in moderate-Reynolds number shear flow. *J. Fluid Mech.* **101**, 721–735.

KOTANSKY, D. R. 1966 The use of honeycomb for shear flow generator. *AIAAJ.* **4**, 1490–1491.

LEVI, E. 1980 Three-dimensional wakes: origin and evolution. *Proc. ASCM: J. Engng Mech. Div.* **106**, 659–676.

MAGARVEY, R. H. & BISHOP, R. L. 1961 Transition ranges for three-dimensional wakes. *Can. J. Phys.* **39**, 1418–1422.

MAGARVEY, R. H. & MACLATCHY, C. S. 1965 Vortices in sphere wakes. *Can J. Phys.* **43**, 1649–1656.

MODI, V. J. & AKUTSU, T. 1984 Wall confinement effects for spheres in the Reynolds number range of 30–2000. *Trans. ASME* I: *J. Fluids Engng* **106**, 66–73.

MÖLLER, W. 1938 Experimentelle untersuchung zur hydromechanik der kugel. *Phys. Zeitschrift* **39**, 57–80.

MORKOVIN, M. V. 1964 Flow around circular cylinder – A kaleidoscope of challenging fluid phenomena. *Symp. on Fully Separated Flows* (ed. A. G. Hansen), pp. 102–118. New York: ASME.

O'NEILL, M. E. 1968 A sphere in contact with a plane wall in a slow linear shear flow. *Chem. Engng Sci.* **23**, 1293–1298.

OWEN, P. R. & ZIENKIEWICZ, H. K. 1957 The production of uniform shear flow in a wind tunnel. *J. Fluid Mech.* **2**, 521–531.

PAO, H. P. & KAO, T. W. 1977 Vortex structure in the wake of a sphere. *Phys. Fluids* **20**, 187–191.

PERRY, A. E. & LIM, T. T. 1978 Coherent structures in coflowing jets and wakes. *J. Fluid Mech.* **88**, 451–463.

PERRY, A. E. & WATMUFF, J. F. 1981 The phase-averaged large-scale structures in three-dimensional turbulent wakes. *J. Fluid Mech.* **103**, 33–51.

PRUPPACHER, H. R., LE CLAIR, B. P. & HAMIELEC, A. E. 1970 Some relations between drag and flow pattern of viscous flow past a sphere and a cylinder at low and intermediate Reynolds numbers. *J. Fluid Mech.* **44**, 781–790.

SAFFMAN, P. G. 1965 The lift on a small sphere in a slow shear flow. *J. Fluid Mech.* **22**, 385–400.

SAKAMOTO, H. & HANIU, H. 1990 A study on vortex shedding from spheres in a uniform flow. *Trans. ASME* I: *J. Fluids Engng* **112**, 386–392.

ROSHKO, A. 1956 On the development of turbulent wakes from vortex streets. *NACA Rep.* 1191.

ROSHKO, A. 1976 Structure of turbulent shear flow: a new look. *AIAAJ.* **14**, 1349–1357.

TANEDA, S. 1956 Experimental investigation of the wake behind cylinders and plates at low Reynolds numbers. *J. Phys. Soc. Japan* **11**, 302–307.

TANEDA, S. 1978 Visual observations of the flow past a sphere at Reynolds numbers between $10^4$ and $10^6$. *J. Fluid Mech.* **85**, 187–192.

WILLIAMSON, C. H. K. 1989 Oblique and parallel modes of vortex shedding in the wake of a circular cylinder at low Reynolds numbers. *J. Fluid Mech.* **206**, 579–627.

WOO, H. G. C. & CERMAK, J. E. 1992 The production of constant-shear flow. *J. Fluid Mech.* **234**, 279–296.